ACS Photonics

pubs.acs.org/journal/apchd5

Article

Photon Recycling in $CsPbBr_3$ All-Inorganic Perovskite Nanocrystals

Marco van der Laan, Chris de Weerd, Lucas Poirier, Oscar van de Water, Deepika Poonia, Leyre Gomez, Sachin Kinge, Laurens D. A. Siebbeles, A. Femius Koenderink, Tom Gregorkiewicz, and Peter Schall*

Cite This: *ACS Photonics* 2021, 8, 3201−3208

Read Online

ACCESS | Metrics & More | Article Recommendations | Supporting Information

ABSTRACT: Photon recycling, the iterative process of re-absorption and re-emission of photons in an absorbing medium, can play an important role in the power-conversion efficiency of photovoltaic cells. To date, several studies have proposed that this process may occur in bulk or thin films of inorganic lead-halide perovskites, but conclusive proof of the occurrence and magnitude of this effect is missing. Here, we provide clear evidence and quantitative estimation of photon recycling in $CsPbBr_3$ nanocrystal suspensions by combining measurements of steady-state and time-resolved photoluminescence (PL) and PL quantum yield with simulations of photon diffusion through the suspension. The steady-state PL shows clear spectral modifications including red shifts and quantum yield decrease, while the time-resolved measurements show prolonged PL decay and rise times. These effects grow as the nanocrystal concentration and distance traveled through the suspension increase. Monte Carlo simulations of photons diffusing through the medium and exhibiting absorption and re-emission account quantitatively for the observed trends and show that up to five re-emission cycles are involved. We thus identify 4 quantifiable measures, PL red shift, PL QY, PL decay time, and PL rise time that together all point toward repeated, energy-directed radiative transfer between nanocrystals. These results highlight the importance of photon recycling for both optical properties and photovoltaic applications of inorganic perovskite nanocrystals.

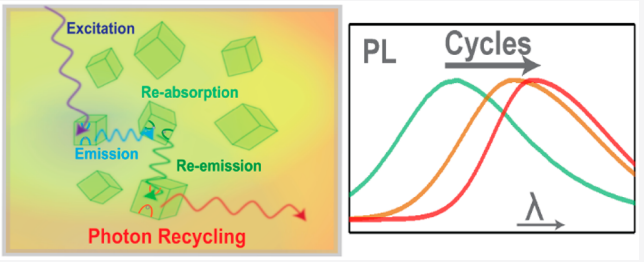

KEYWORDS: *Optoelectronics, Perovskite nanocrystals, Photon recycling, Photoluminescence, Monte Carlo simulation*

Metal halide semiconductors with the perovskite crystal structure have made a major breakthrough since 2009, when they were first applied in photovoltaic (PV) devices processed from solution inks.[1] The optimal range of band gap energy values, high emission efficiencies, and good carrier mobility make them very suitable for PV and optoelectronic applications. Recently reaching conversion efficiencies more than 21%, the perovskite-based PV solar cells are now directly competing with the mainstream multi-crystalline silicon devices.[2] The wet-chemical synthesis fabrication method of perovskite materials offers a fast, cheap, and straightforward production at the 50−200 °C temperature range.[3−5]

So far, most of the research effort has been focused on hybrid organic-inorganic perovskites (e.g., $CH_3CH_3PbI_3$, $CH_3NH_3PbI_3$, etc.) with the general formula $APbX_3$, where the A stands for a cation organic group and X is a halide atom (Cl, Br, or I). These materials feature band gap energies in the 1.5−2.5 eV range, depending on the halide composition, which makes them suitable for both single junction solar cells as well as for top cells in tandems.[6,7] However, for large-scale deployment in PV applications, excellent long-term (chemical and structural) stability under extreme operating conditions is necessary. This is not yet the case for hybrid perovskites which currently suffer from degradation upon light/environmental exposure.[8] The advent of all-inorganic perovskite nanocrystals (IP NCs) of $CsPbX_3$ provides a material free from the organic component,[4] which promises better stability. These NCs combine the advantages of perovskites, low-temperature, and low-cost production as well as band gap tuning by composition, with the typical NC features induced by quantum confinement, i.e., band gap tunability by size and the possibility of surface functionalization.[4,9,10] Consequently, IP NCs feature outstanding optical properties which makes them very attractive materials for solar cells, light detectors, LEDs, and lasers. Recent demonstrations of a stable prototype solar cell based on $CsPbI_3$ NCs promote IP NCs as an attractive candidate for development of the next-generation, high-efficiency photovoltaic devices.[11]

Photon recycling (PR) is an iterative process of multiple self-absorption and re-emission events of photons within the excited material. Originally identified in GaAs, it was subsequently observed in several other direct-band-gap semiconductors[12−15] and found to be the main factor in the difference in maximum achievable efficiencies in *pn*-junction

Received: June 25, 2021
Published: October 18, 2021

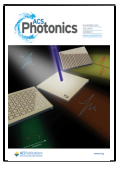

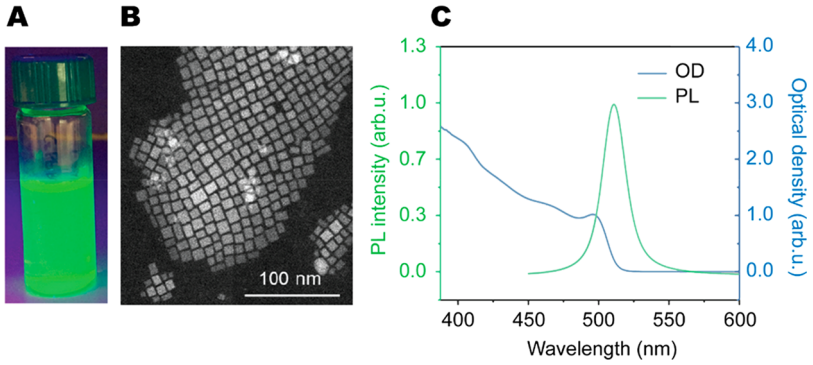

Figure 1. Optical characterization. (A) The sample illuminated by a UV lamp (λ_{exc} = 365 nm). (B) STEM image of fresh drop-casted $CsPbBr_3$ NCs, revealing an average size of 10.2 ± 1.8 nm. (C) PL (green) and optical density (blue) showing the overlap between the PL maximum and the absorption onset.

solar cells as calculated from Shockley's diode's equation and the detailed balance model of Shockley and Queisser, where neglecting photon recycling results in lower efficiencies.[16] This suggests that, to realize high solar cell efficiencies, materials with strong photon recycling should be selected.[17]

In view of their high photoluminescence quantum yield (PL QY) and large absorption cross section, one may expect that PR takes place in perovskites also, but dispute about the occurrence and magnitude of this effect is ongoing. Efficient photon re-absorption was reported in $CH_3NH_3PbI_3$ and $CH_3NH_3PbBr_3$ bulk perovskite single crystals,[18,19] and the full cycle of re-absorption and re-emission in perovskite materials was investigated in thin films of the hybrid lead-iodide perovskite.[20] However, while the variation of PL intensity with distance from the surface suggested the presence of PR,[21,22] other work argued that the PR-related component constituted only approximately 0.5% of the total external emission, and the observed PL intensity gradient arises due to the long intrinsic carrier diffusion lengths.[23] Additional work performed on photon recycling in $CsPbBr_3$-based or 2D perovskite waveguides showed repeated photoluminescence spectral and lifetime changes with increasing distance between excitation and detection.[24−26] Colloidal suspensions of perovskite NCs offer to further resolve the ongoing dispute as carrier diffusion is totally inhibited. Moreover, the absorption cross section near the NC band gap is typically much larger than that of the bulk, which provides yet additional advantage.[27] Evidence of radiative energy transfer was indeed obtained in mixtures of $CsPbCl_3$ and $CsPbI_3$ NCs,[28] where photons emitted by the larger-band-gap $CsPbCl_3$ NCs were re-absorbed and re-emitted by the smaller-band-gap $CsPbI_3$ NCs. Within a single NC ensemble, however, the occurrence of PR is unclear: it was inferred from the apparent Stokes shift in NC dispersions,[29] and carrier diffusion lengths in NC films,[30] but despite its importance for PV applications, a clear proof and quantitative determination of PR is missing. NC dispersions would provide the most unambiguous proof of photon recycling, as other forms of energy transport, notably carrier diffusion, are minimized, and NC concentrations can be varied easily, allowing for systematic exploration of the PR effect.

Here, we provide conclusive proof of efficient PR in colloidal dispersions of $CsPbBr_3$ NCs and present a quantitative measure of the effect in terms of the number of re-absorption and re-emission cycles. We combine measurements of steady-state and time-dependent PL and PLQY of IP NC solutions with dedicated Monte Carlo simulations of the photon scattering, absorption, and re-emission processes, while varying the NC concentration and distance traveled through the suspension. This allows us to identify characteristic concomitant changes in the spectra, PLQY, and PL rise and decay times that can only be accounted for if re-emission of photons is included in the Monte Carlo simulations. In particular, the unusual simultaneous decrease of PLQY and increase of PL lifetime with NC concentration clearly indicates that an energy transfer mechanism via absorption and re-emission takes place, and comparison with simulations shows that as many as 5 re-emission events underlie these experimentally observed trends. Hence, our results pinpoint the photon recycling process quantitatively and demonstrate its crucial importance for the optical properties of IP NCs. When taken together with the well-known excellent optical properties, these results identify IP NCs as an ideal candidate material for development of the next generation of highly efficient and mechanically flexible thin-film solar cells.

EXPERIMENTAL SECTION

$CsPbBr_3$ NCs were synthesized following the protocol reported by Protesescu et al. with some modifications; see the Supporting Information (SI) for details.[4] The final product, referred to as Dilution 1, had a concentration of 85 mg/mL in toluene and a measured PL QY of 90% in the dilute limit. Further dilutions of 2, 5, 10, 25, and 50 times were prepared by adding the appropriate amount of toluene. The optical density was measured in a LAMBDA 950 UV/vis/NIR spectrophotometer (PerkinElmer), using a combination of a tungsten-halogen and deuterium lamp providing a spectral range of 300−800 nm. Sample and solvent measurements were performed separately and subtracted from each other. The PL spectra were recorded in a right-angle geometry by a CCD camera after sample excitation with 490 nm pulses from an optical parametric oscillator (OPO) pumped by a Nd:YAG laser. The distance between the excitation and collection spots was varied over the full length of the quartz cuvette containing the NC suspensions. For the PL QY and time-resolved photoluminescence (TRPL) measurements, $CsPbBr_3$ nanocrystals from a different batch were used with measured PL QY of around 55% in the dilute limit. The PL QY was determined using an integrating sphere with a 150 W xenon lamp coupled to a spectrometer (Solar, MSA-130) as excitation source. The emission light and excitation light were scattered diffusively in the integrating sphere and detected with a CCD (Hamamatsu S10141-1108S) coupled to another spectrometer (Solar,

https://doi.org/10.1021/acsphotonics.1c00953
ACS Photonics 2021, 8, 3201−3208

M266). The TRPL measurements are performed using a LifeSpec II time-correlated single photon counting (TCSPC) spectrometer (Edinburgh Instruments) with a 230−850 nm detection range (MCP-PMT). A diode laser with an excitation wavelength of 375 nm (EPL series) provides a 100 ps pulse. A right angle between the excitation and emission beam paths is maintained to avoid detecting scattered excitation light.

EXPERIMENTAL RESULTS

Preliminaries. The optical characteristics of the undiluted IP-NC colloid are shown in Figure 1. As can be inferred from the comparison of the presented spectra, there is a clear overlap between the PL band, peaking around 510 nm, and the absorption featuring an excitonic peak at the onset. This reflects the relatively narrow size distribution of IP NCs of the investigated ensemble, but also the enhanced absorption cross section for the close-to-band-gap excitation. Figure 1B shows a HRTEM image of the colloid when drop-casted onto a carbon grid into a single NC layer; the characteristic nanocubes, with an edge size of around 10 nm, are readily recognized.

To investigate photon recycling, we prepare suspensions of different concentrations of IP NCs by appropriate dilution of the original suspension. We measure the PL intensity, spectrum, and decay time for different IP NC concentrations as a function of the distance between excitation and emission collection spots. The experimental setup is illustrated in Figure 2. A thin quartz cuvette is excited from the side with a laser

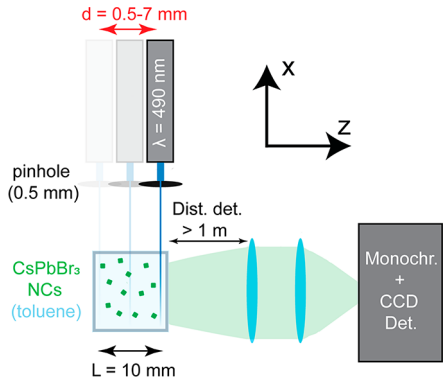

Figure 2. Schematics of the experimental setup. The cuvette is excited while maintaining a 90° angle between excitation (λ_{exc} = 490 nm) and collection (by the CCD) to avoid detecting the excitation pulse directly. The cuvette is mounted on a moveable stage such that the distance d, i.e., the distance between the excitation and emission window, can be varied between 0.5 and 7 mm by moving the cuvette in the z-direction. The maximum distance between excitation and collection is fixed. The distance from the cuvette to the collimating lenses is chosen to be much greater than the cuvette length to avoid significant changes in the detection NA upon moving the cuvette.

with excitation wavelength λ_{exc} = 490 nm passing through a pinhole, fixing the excitation spot diameter at 0.5 mm. The emerging PL is collected from the front of the cuvette and projected through a set of lenses onto the fiber coupler and further to a spectrometer equipped with a CCD camera for detection. The 90° angle configuration has been chosen to avoid detecting the excitation light directly. The cuvette is mounted on a movable stage, such that the distance d between the excitation spot and the emission collection window can be modified between 0.5 and 7 mm. Since the focal length of the detection lenses is much larger than the maximum cuvette shift, the PL collection cone is practically fixed. This geometry should result in minimal change in PL intensity upon varying d for a dilute sample, which was indeed verified for a colloid with low optical density, for which the re-absorption of the emitted light was negligible.

Upon excitation, photons emitted (isotropically) by the NCs propagate through the NC suspension and can be scattered out of the cuvette or re-absorbed by other NCs. The situation changes under conditions of strong re-absorption and high PL QY: in that case, (some of) the NCs excited by emitted photons from other NCs, can re-emit photons, again isotropically. This photon recycling process changes the spectral characteristics. In particular, it suppresses the number of high-energy photons in the collected PL spectrum, which becomes asymmetric and shifts to the red, as the larger NCs, having a larger excitation cross section, will be preferentially re-excited at the expense of the high-energy photons emitted by smaller NCs. We then expect that the actual magnitude of this red shift will increase with NC concentration, and the distance d. Moreover, the re-excitation of larger NCs will increase the effective decay time of their population. Further, we can expect that an efficient photon recycling process will affect the PL intensity dependence on distance d and lower the number of emitted photons arriving at the detector, resulting in a reduced apparent PL QY.

Spectral Modification. PL spectra of the differently concentrated NC solutions—ranging from 2 up to 50 times diluted—measured for three excitation-collection distances are shown in Figure 3A−C. The data have been normalized to best

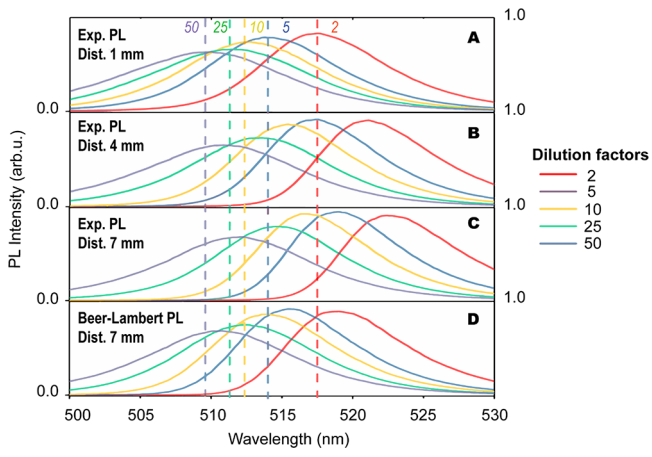

Figure 3. The spectral changes induced by photon recycling. (A−C) Normalized PL spectra, varying d between 1 and 7 mm. Dilution factor (colors) indicates the degree of dilution where a dilution factor of 1 refers to the as-synthesized sample. The vertical dashed lines indicate peak positions of the spectra at a distance of 1 mm. (D) The Beer−Lambert prediction (normalized) for the sample with dilution factor 5. The experimental data show increased spectral change as compared to the Beer−Lambert prediction, indicating that the simple process of re-absorption without taking into account strong scattering or re-emission is not sufficient to explain the experimental data.

visualize the modification of the shape of the PL spectra. For the smallest separation, d = 1 mm (Figure 3A), we observe merely a small red shift, whose magnitude increases with NC concentration. The red shift becomes more pronounced, however, if d is increased to 4 mm (Figure 3B). Both features, red shift and spectral asymmetry, are very pronounced for d = 7 mm (Figure 3C). For an easy comparison, in the bottom

https://doi.org/10.1021/acsphotonics.1c00953
ACS Photonics 2021, 8, 3201−3208

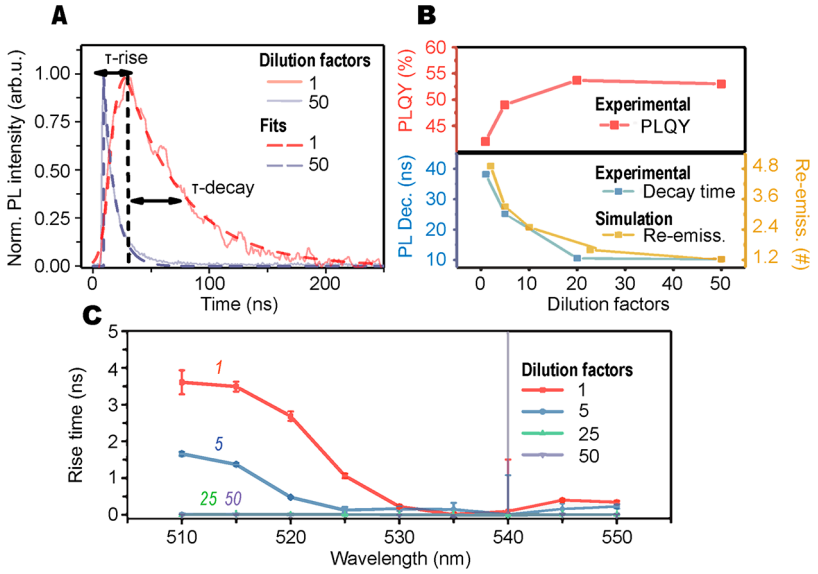

Figure 4. Time-resolved photoluminescence and photoluminescence quantum yield data for various dilutions. (A) Two example traces (solid) and their fits (dashed) for the most diluted (purple) and most concentrated (red) sample on a linear scale. The curves have been normalized to show the differences between these data sets. Most notably, the decay time of the less-diluted sample is longer but still well-fitted by a single exponent. In addition, there is a slight rise time visible for the more concentrated sample. (B) Comparison between experimental PLQY (red), TRPL decay times (blue), and simulated re-emission events (gold), as a function of dilution. The magnitude of these simulated events has been scaled such that the data point for the most diluted sample overlaps with the corresponding TRPL point. (C) Fitted rise times from TRPL traces as a function of detected photon wavelength for various sample dilutions. Clearly, the more concentrated samples show a rise time, for short-wavelength photons, whereas the diluted samples do not. This evidences indirect excitations in the concentrated samples. The larger increase of the rise time at shorter wavelengths can be attributed to strong re-absorption and consequently a lower probability detection of photons generated from direct laser excitation.

panel of Figure 3, we present how the PL spectrum should change with the distance d if spectral attenuation occurs as modeled by the Beer–Lambert law. In this case, the distance-dependent intensity $I_d(\lambda) = I_0(\lambda)\exp[-\mu(\lambda)d]$, where μ is the (wavelength-dependent) attenuation coefficient. In practice, the re-absorption-free spectrum $I_0(\lambda)$ was obtained for highly diluted colloids and represents the "unfiltered" and "un-recycled" emission spectrum; as can be anticipated, in this case, the spectrum is independent of the distance d.

Clearly, the measured PL spectra are remarkably different from those corrected using the Beer–Lambert law and given in the bottom panel of Figure 3. In particular, the much stronger measured red shift suggests that simple re-absorption alone is not sufficient to account for the observed modification of the PL spectra and that additional processes must play a role. Detailed investigation of the distance and dilution dependence of both the PL peak intensities and the PL peak position confirms this conclusion; see the SI. In all cases, there is a clear discrepancy between experiment and Beer–Lambert prediction, with the experiment revealing a considerably stronger PL red shift than the Beer–Lambert simulated one. Similar spectral changes were also observed in drop-casted $MAPbBr_3$ nanocrystal films, $CsPbBr_3$ microwires, and $CsPbBr_3$ nanocrystal film waveguides,[24,26,30] showing their dominance in these perovskite nanocrystal materials.

PL Dynamics and PL QY. A signature of additional processes is also observed in the PL decay time and its concentration dependence. Examples of the experimental and fitted time-dependent PL traces are shown in Figure 4A. In all cases, the data are well fitted with a single exponential decay, resulting in approximately 10 and 40 ns decay times for the lowest and highest concentrated samples, respectively. The range of these values is consistent with previous reports in the literature; see, for example, the work of Protesescu et al.[4] Remarkably, Figure 4A shows strong characteristic differences between the dilutions, most notably the longer decay times, as well as the emergence of a rise time for samples of higher concentration. These phenomena are clearly visible in the full concentration dependence of the PL decay and rise times as shown in panels B and C.

The PL decay times as a function of dilution (Figure 4B bottom, left axis) show that, for higher NC concentrations, the decay times consistently increase. In the same panel (top), we also plot the experimental PLQY values for these sample dilutions. The two data sets show inverse trends, with PLQY values decreasing and PL decay times increasing with concentration. Normally, we would expect that PLQY values and PL decay times show similar trends due to the competition between radiative and non-radiative rates; thus longer decay times will lead to higher PLQY due to the absence of non-radiative channels. However, the opposite is observed here. From the inverse trends of the PL decay time and PLQY, we conclude that these changes are not due to changes of the intrinsic radiative and non-radiative rates, but rather indicate a delay and concomitant efficiency loss associated with energy transfer events relating to PR events.

Since the PR is an energy-exchange process encompassing photon emission and re-absorption between two NCs, it should not affect the (effective) lifetime of the "donor" NC. On the "acceptor" NC side, photon re-absorption induces a delayed excitation; the latter should lead to a prolongation of the decay as is indeed observed. As can be concluded from Figure 4B, the PL decay in a concentrated sample is more than 4 times longer in a more diluted sample, where PR is quenched. At the same time, we note that the ~10 ns decay time measured for the PR-free sample agrees well with values

https://doi.org/10.1021/acsphotonics.1c00953
ACS Photonics 2021, 8, 3201–3208

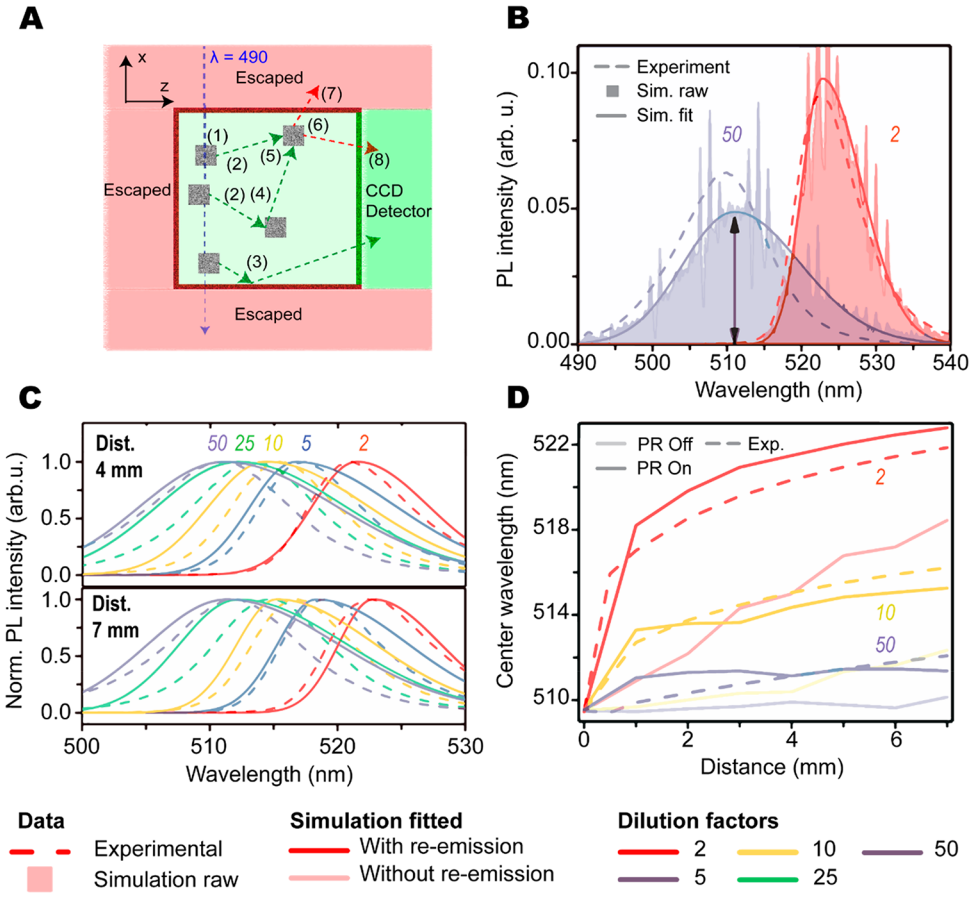

Figure 5. Comparison of simulated spectra with experimental spectra. (A) Schematic description of the model with most notably the processes of scattering (4), absorption (5), and re-emission (6) included; for more details, see the SI. (B) An example overview of modeled spectra (filled curves), their fits (solid curves), and experimental data (dashed curves) for the two extreme cases of high-dilution-short-distance (purple) and low-dilution-large-distance (red). While the simulations do not fully accurately reproduce the experimental data, clearly a red shift can be captured in the simulations. For more details on the choices of simulation parameters, see the SI. (C) Comparison of the experimental spectra (dashed lines) and fitted simulated spectra (solid lines) for 2 excitation-detection distances and various dilutions. (D) Center wavelengths of the fitted experimental (dashed) and simulated (solid) curves. In the simulations, a distinction is made between recycling On (dark/solid lines) and Off (light/transparent lines). In this panel, the center wavelengths are displayed as a function of distance for three different NC dilutions. This last panel shows that the simulations follow the experiment more closely when re-emission is taken into account (recycling On).

determined for single NCs (~6−10 ns),[31] which represents an intrinsic decay time for IP NCs. This large delay of the PL decay, combined with the systematic decrease of the PLQY, provides a powerful evidence of PR.

The photon recycling process is further substantiated in the PL rise times, plotted as a function of photon wavelength in Figure 4C. Apparently, for concentrated samples, the rise time increases significantly, up to almost 4 ns for shorter wavelength, whereas, for more dilute samples, no significant rise times are observed for any photon wavelength. As laser excitation and photon travel over the experimental distances can be considered instantaneous, the dilution dependence of the rise times can only be explained by the occurrence of indirect excitations in the more concentrated samples. The wavelength dependence can then be well understood from the fact that it is more likely for short-wavelength photons to be re-absorbed. Indeed, the wavelength range where the rise time becomes pronounced corresponds well with the absorption onset shown in Figure 1C. Evidently, to be able to measure any photons from indirectly excited NCs, these NCs must re-emit as well; therefore, the occurrence of a rise time in the TRPL traces is another indication of the photon recycling process. Indeed, measurements on waveguides of low-dimensional perovskites show a qualitatively similar increase of photoluminescence rise times with increasing excitation-detection distance, conceptually consistent with the dilution-dependent rise times presented here.[24−26]

We thus observe clear indications of photon recycling: both the increasing PL red shift and asymmetry for increasing excitation-detection distances and sample concentrations, which are not adequately modeled by Beer−Lambert predictions, as well as the longer PL decay and rise times for concentrated samples indicate ubiquitous transfer processes consistent with PR. In addition, the inverse trend of PL decay time and PLQY gives further support that an effect other than an intrinsic change of the PL mechanism of the NCs underlies the observed trends.

Random Walk Simulations. To further substantiate these results and obtain insight into the re-absorption and re-emission processes, we perform Monte Carlo simulations of random photon walks in a 2D cuvette as illustrated in Figure 5A. After initial excitation (1), photons are emitted in random directions (2), taking a step with size defined by their mean-free-path length. The photons can subsequently undergo

https://doi.org/10.1021/acsphotonics.1c00953
ACS Photonics 2021, 8, 3201−3208

reflection (3), scattering (4), absorption (5), and re-emission (6) before escaping the boundaries of the simulated cuvette (7) or being detected (8). These simulations are run for various excitation-detector distances and dilutions, with 10^6 photons for each simulation. To distinguish the effects of mere re-absorption and scattering from those of re-emission, the simulations allow for turning the PR process on or off by choosing to include re-emission or not. The simulations are calibrated from transmission measurements, providing the wavelength-dependent mean free path, the associated optical path length distribution width, and an estimate of the relative probabilities of absorption versus scattering. The microscopic Stokes shift is used as a free adjustable parameter and was optimized to be 4 nm, but also values in a wider range of 2−5 nm yield reasonable agreement with the measurements, as detailed in the SI.

Simulated PL spectra are shown together with the corresponding experimental spectra in Figure 5B,C. In Figure 5C, we compare measurements (dashed lines) and simulation results (shaded area and solid line) for two extreme cases: the most diluted sample excited 1 mm from the detector edge of the cuvette (left, blue), and the most concentrated sample, excited at 7 mm from the detector edge (right, red). We then fit the peak of each simulated spectrum with half-Gaussian functions according to the peak widths on both sides, and with the same center energy, peak amplitude and background level. Close correspondence with the experimental data is observed, though some deviation is visible for the diluted sample. A more detailed comparison for a wider range of data sets using the fitted simulation results is provided in Figure 5C and SI Figure S2. For both excitation-detector distances, overall good agreement is observed, given the simplicity of the two-dimensional model. The observed red shifts follow closely those observed in experiments, unlike the Beer−Lambert predictions in Figure 3D. Furthermore, from the fitted simulated and experimental spectra, we extract the center wavelength and compare their shift as a function of excitation-detection distance, solid and dashed lines, in Figure 5D. To clearly demonstrate the PR effect, we also include simulation results without re-emission, i.e., with PR turned off; see faint solid lines. Clearly, without PR, the simulations do not capture the observed trends of a strong peak shift increasing with distance and concentration. With re-emission in contrast, the simulations follow closely the experimental trends for all dilutions; the deviation for the closest excitation-detector distance at highest dilution can be explained by the two-dimensional simulation geometry, capturing re-emitted photons more efficiently than in a three-dimensional geometry. Even in this most dilute sample, however, some re-emission is needed to provide good correspondence with the experimental data. Similar conclusions with much stronger trends can be drawn for the more concentrated samples, evidencing the occurrence of the PR process.

Number of Recycling Events and PL Dynamics. We can now use the simulations to estimate the number of recycling events underlying the spectral shifts observed experimentally. To do so, for each dilution, we determine the average number of re-emission events from the simulation runs, and we overlay this number as a function of dilution onto the PL decay times from experiments in Figure 4B (gold color, right axis). A remarkable consistency is observed, indicating that the longer decay times can indeed be accounted for by repeated re-absorption and emission events. In the most concentrated samples, the average number of re-emission events is ∼5, decreasing toward 1 as the sample is diluted. Thus, we conclude that as many as 5 recycling events underlie the strong red shift and concomitant time delay observed in the experiments. Obviously, if re-emission is turned off in the simulations, no such correspondence with experimental PL decay times can be observed. Therefore, the PR process causes these trends in the measured PL decay times, leading to a concomitant decrease of the PL QY. We note that the highest average number of recycling events in the concentrated colloid is roughly consistent with a 1D Monte Carlo approach for $CsPbBr_3$ waveguides reported in the literature.[30] However, in such solid sample geometries, additional carrier transport takes place, which could affect how much of the apparent carrier diffusion lengths can be attributed to photon recycling.

Finally, we note that, even though the data from simulations and experiments consistently point toward radiative transfer in the form of photon recycling, in principle, one might argue that some other, alternative, transport and transfer process could also underlie the trends in the optical data. Notably, transfer in the form of diffusion together with energy transfer between close NCs could, in principle, qualitatively account for the observed trends. However, as we show in the SI, the typical diffusion distance covered within the characteristic time scale of 10 ns (PL decay time) is several orders of magnitude too small to encounter any significant number of other NCs for energy transfer, thus ruling out this diffusive mechanism. This again suggests that it is indeed radiative transfer, i.e., photon recycling, which underlies the observed trends.

CONCLUSIONS

We have shown that photon recycling leads to a characteristic red shift, systematic increase of PL rise and decay times, and lowering of the PLQY in colloidal solutions of inorganic lead-halide perovskite NCs. While earlier studies could not properly distinguish between signatures of carrier diffusion and photon diffusion, for the thin film or bulk cases, in this study, we have used well-dispersed nanocrystals ruling out such carrier diffusion. We observed distinct trends in the optical emission such as PL red shift, PL asymmetry, PLQY, and PL rise and decay times that are characteristic of photon recycling. Furthermore, simulated PL spectra based on random photon walks allow distinction of (re-)absorption and scattering effects from those relating to re-emission. This leads us to the conclusion that the observed trends in the PL spectra are due to photon recycling. The surprisingly large number of re-emission cycles highlights the importance of PR for these IP NCs, their optical properties, and PV device performance. Since for NC ensembles, energy transfer, including photon re-absorption, generally proceeds from smaller to larger NCs, one can speculate that the PR phenomenon could be explored toward directional funneling of energy and carriers to improve, e.g., photon and carrier extraction in devices. Furthermore, to generalize these findings to nanocrystal films and future devices, the 2D Monte Carlo simulation could be extended to include carrier transport as well. In a first approximation, this could be modeled by allowing for spatially separated re-absorption and re-emission events. The numerical nature of a Monte Carlo simulation facilitates quantification of the competition between the various optical and carrier processes over more analytical approaches. We conclude that IP NCs have a huge potential for future solar cells, featuring uniquely efficient photon recycling in addition to other, well-known

https://doi.org/10.1021/acsphotonics.1c00953
ACS Photonics 2021, 8, 3201−3208

advantages of facile low-temperature synthesis, direct band gap, defect tolerance, and long carrier lifetime.

■ ASSOCIATED CONTENT

Supporting Information

The Supporting Information is available free of charge at https://pubs.acs.org/doi/10.1021/acsphotonics.1c00953.

Synthesis details; Monte Carlo simulation design; simulation parameter tests; time-resolved photoluminescence fitting details; complete set of experimental and simulated photoluminescence spectral; estimation of nanocrystal Brownian motion (PDF)

■ AUTHOR INFORMATION

Corresponding Author

Peter Schall − *Institute of Physics, University of Amsterdam, 1098 XH Amsterdam, The Netherlands*; Email: P.Schall@uva.nl

Authors

Marco van der Laan − *Institute of Physics, University of Amsterdam, 1098 XH Amsterdam, The Netherlands;* orcid.org/0000-0001-9571-3190

Chris de Weerd − *Institute of Physics, University of Amsterdam, 1098 XH Amsterdam, The Netherlands;* orcid.org/0000-0002-8826-2616

Lucas Poirier − *Institute of Physics, University of Amsterdam, 1098 XH Amsterdam, The Netherlands;* Present Address: Advanced Research Center for Nanolithography, Science Park 106, 1098 XG Amsterdam, The Netherlands

Oscar van de Water − *Institute of Physics, University of Amsterdam, 1098 XH Amsterdam, The Netherlands*

Deepika Poonia − *Optoelectronic Materials Section, Department of Chemical Engineering, Delft University of Technology, 2629 HZ Delft, The Netherlands*

Leyre Gomez − *Institute of Physics, University of Amsterdam, 1098 XH Amsterdam, The Netherlands; Catalan Institute of Nanoscience and Nanotechnology, CSIC, BIST, and CIBERBBN, 08193 Barcelona, Spain;* orcid.org/0000-0002-2926-5665

Sachin Kinge − *Optoelectronic Materials Section, Department of Chemical Engineering, Delft University of Technology, 2629 HZ Delft, The Netherlands; Materials Research & Development, Toyota Motor Europe, B1930 Zaventem, Belgium*

Laurens D. A. Siebbeles − *Optoelectronic Materials Section, Department of Chemical Engineering, Delft University of Technology, 2629 HZ Delft, The Netherlands;* orcid.org/0000-0002-4812-7495

A. Femius Koenderink − *Institute of Physics, University of Amsterdam, 1098 XH Amsterdam, The Netherlands; Center for Nanophotonics, AMOLF, 1098 XG Amsterdam, The Netherlands;* orcid.org/0000-0003-1617-5748

[▽]**Tom Gregorkiewicz** − *Institute of Physics, University of Amsterdam, 1098 XH Amsterdam, The Netherlands*

Complete contact information is available at: https://pubs.acs.org/10.1021/acsphotonics.1c00953

Notes

The authors declare no competing financial interest.

[▽]Tom Gregorkiewicz is deceased, July 7, 2019.

■ ACKNOWLEDGMENTS

We would like to thank Dr. Antonio Capretti (University of Amsterdam) for his involvement and for his contribution to discussions on this research. This research received funding from The Netherlands Organisation for Scientific Research (NWO) in the framework of the Materials for Sustainability Programme (MAT4SUS Project No. 739.017.011).

■ REFERENCES

(1) Kojima, A.; Teshima, K.; Shirai, Y.; Miyasaka, T. Organometal halide perovskites as visible-light sensitizers for photovoltaic cells. *J. Am. Chem. Soc.* **2009**, *131* (17), 6050−6051.

(2) Green, M. A.; Dunlop, E. D.; Hohl-Ebinger, J.; Yoshita, M.; Kopidakis, N.; Hao, X. Solar cell efficiency tables (version 56). *Prog. Photovoltaics* **2020**, *28*, 629−638.

(3) Heo, J. H.; Song, D. H.; Im, S. H. Planar $CH_3NH_3PbBr_3$ hybrid solar cells with 10.4% power conversion efficiency, fabricated by controlled crystallization in the spin-coating process. *Adv. Mater. (Weinheim, Ger.)* **2014**, *26* (48), 8179−8183.

(4) Protesescu, L.; Yakunin, S.; Bodnarchuk, M. I.; Krieg, F.; Caputo, R.; Hendon, C. H.; Yang, R. X.; Walsh, A.; Kovalenko, M. V. Nanocrystals of cesium lead halide perovskites ($CsPbX_3$, X= Cl, Br, and I): novel optoelectronic materials showing bright emission with wide color gamut. *Nano Lett.* **2015**, *15* (6), 3692−3696.

(5) Jeon, N. J.; Noh, J. H.; Kim, Y. C.; Yang, W. S.; Ryu, S.; Seok, S. I. Solvent engineering for high-performance inorganic−organic hybrid perovskite solar cells. *Nat. Mater.* **2014**, *13* (9), 897−903.

(6) Mosconi, E.; Umari, P.; De Angelis, F. Electronic and optical properties of $MAPbX_3$ perovskites (X= I, Br, Cl): a unified DFT and GW theoretical analysis. *Phys. Chem. Chem. Phys.* **2016**, *18* (39), 27158−27164.

(7) Eperon, G. E.; Leijtens, T.; Bush, K. A.; Prasanna, R.; Green, T.; Wang, J. T. W.; McMeekin, D. P.; Volonakis, G.; Milot, R. L.; May, R.; Palmstrom, A.; et al. Perovskite-perovskite tandem photovoltaics with optimized band gaps. *Science* **2016**, *354* (6314), 861−865.

(8) McLeod, J. A.; Liu, L. Prospects for mitigating intrinsic organic decomposition in methylammonium lead triiodide perovskite. *J. Phys. Chem. Lett.* **2018**, *9* (9), 2411−2417.

(9) Nedelcu, G.; Protesescu, L.; Yakunin, S.; Bodnarchuk, M. I.; Grotevent, M. J.; Kovalenko, M. V. Fast anion-exchange in highly luminescent nanocrystals of cesium lead halide perovskites ($CsPbX_3$, X= Cl, Br, I). *Nano Lett.* **2015**, *15* (8), 5635−5640.

(10) Li, X.; Wu, Y.; Zhang, S.; Cai, B.; Gu, Y.; Song, J.; Zeng, H. $CsPbX_3$ quantum dots for lighting and displays: room-temperature synthesis, photoluminescence superiorities, underlying origins and white light-emitting diodes. *Adv. Funct. Mater.* **2016**, *26* (15), 2435−2445.

(11) Sanehira, E. M.; Marshall, A. R.; Christians, J. A.; Harvey, S. P.; Ciesielski, P. N.; Wheeler, L. M.; Schulz, P.; Lin, L. Y.; Beard, M. C.; Luther, J. M. Enhanced mobility $CsPbI_3$ quantum dot arrays for record-efficiency, high-voltage photovoltaic cells. *Sci. Adv.* **2017**, *3* (10), eaao4204.

(12) Hwang, C. J. Quantum efficiency and radiative lifetime of the band-to-band recombination in heavily doped n-type GaAs. *Phys. Rev. B* **1972**, *6* (4), 1355.

(13) Asbeck, P. Self-absorption effects on the radiative lifetime in GaAs-GaAlAs double heterostructures. *J. Appl. Phys. (Melville, NY, U. S.)* **1977**, *48* (2), 820−822.

(14) Ettenberg, M. The effect of reabsorbed radiation on the minority-carrier diffusion length in GaAs. *Appl. Phys. Lett.* **1977**, *30* (4), 207−210.

(15) Ahrenkiel, R. K.; Dunlavy, D. J.; Keyes, B.; Vernon, S. M.; Dixon, T. M.; Tobin, S. P.; Miller, K. L.; Hayes, R. E. Ultralong minority-carrier lifetime epitaxial GaAs by photon recycling. *Appl. Phys. Lett.* **1989**, *55* (11), 1088−1090.

(16) Martı, A.; Balenzategui, J. L.; Reyna, R. F. Photon recycling and Shockley's diode equation. *J. Appl. Phys. (Melville, NY, U. S.)* **1997**, *82* (8), 4067−4075.

(17) Miller, O. D.; Yablonovitch, E.; Kurtz, S. R. Strong internal and external luminescence as solar cells approach the Shockley−Queisser limit. *IEEE J. Photovolt.* **2012**, *2* (3), 303−311.
(18) Yamada, Y.; Yamada, T.; Phuong, L. Q.; Maruyama, N.; Nishimura, H.; Wakamiya, A.; Murata, Y.; Kanemitsu, Y. Dynamic optical properties of $CH_3NH_3PbI_3$ single crystals as revealed by one- and two-photon excited photoluminescence measurements. *J. Am. Chem. Soc.* **2015**, *137* (33), 10456−10459.
(19) Yamada, T.; Yamada, Y.; Nishimura, H.; Nakaike, Y.; Wakamiya, A.; Murata, Y.; Kanemitsu, Y. Fast Free-Carrier Diffusion in $CH_3NH_3PbBr_3$ Single Crystals Revealed by Time-Resolved One- and Two-Photon Excitation Photoluminescence Spectroscopy. *Adv. Electron. Mater.* **2016**, *2* (3), 1500290.
(20) Pazos-Outon, L. M.; Szumilo, M.; Lamboll, R.; Richter, J. M.; Crespo-Quesada, M.; Abdi-Jalebi, M.; Beeson, H. J.; Vrucinic, M.; Alsari, M.; Snaith, H. J.; Ehrler, B.; Friend, R. H.; Deschler, F. Photon recycling in lead iodide perovskite solar cells. *Science* **2016**, *351* (6280), 1430−1433.
(21) Yamada, T.; Yamada, Y.; Nakaike, Y.; Wakamiya, A.; Kanemitsu, Y. Photon emission and reabsorption processes in $CH_3NH_3PbBr_3$ single crystals revealed by time-resolved two-photon-excitation photoluminescence microscopy. *Phys. Rev. Appl.* **2017**, *7* (1), 014001.
(22) Yamada, T.; Aharen, T.; Kanemitsu, Y. Near-Band-Edge Optical Responses of $CH_3NH_3PbCl_3$ Single Crystals: Photon Recycling of Excitonic Luminescence. *Phys. Rev. Lett.* **2018**, *120* (5), 057404.
(23) Fang, Y.; Wei, H.; Dong, Q.; Huang, J. Quantification of re-absorption and re-emission processes to determine photon recycling efficiency in perovskite single crystals. *Nat. Commun.* **2017**, *8*, 14417.
(24) Dursun, I.; Zheng, Y.; Guo, T.; De Bastiani, M.; Turedi, B.; Sinatra, L.; Haque, M. A.; Sun, B.; Zhumekenov, A. A.; Saidaminov, M. I.; Garcia de Arquer, F. P.; et al. Efficient photon recycling and radiation trapping in cesium lead halide perovskite waveguides. *ACS Energy Lett.* **2018**, *3* (7), 1492−1498.
(25) Zheng, Y.; Naphade, R.; Mondal, N.; Bakr, O. M.; Mohammed, O. F.; Gartstein, Y. N.; Malko, A. V. Light Propagation and Radiative Exciton Transport in Two-Dimensional Layered Perovskite Microwires. *ACS Photonics* **2021**, *8* (1), 276−282.
(26) Navarro-Arenas, J.; Suárez, I.; Gualdrón-Reyes, A. F.; Mora-Seró, I.; Bisquert, J.; Martínez-Pastor, J. P. Recycled Photons Traveling Several Millimeters in Waveguides Based on CsPbBr3 Perovskite Nanocrystals. *Adv. Opt. Mater.* **2021**, *9*, 2100807.
(27) Chen, J.; Zidek, K.; Chabera, P.; Liu, D.; Cheng, P.; Nuuttila, L.; Al-Marri, M. J.; Lehtivuori, H.; Messing, M. E.; Han, K.; Zheng, K.; Pullerits, T. Size-and wavelength-dependent two-photon absorption cross-section of $CsPbBr_3$ perovskite quantum dots. *J. Phys. Chem. Lett.* **2017**, *8* (10), 2316−2321.
(28) Davis, N. J. L. K.; de la Pena, F. J.; Tabachnyk, M.; Richter, J. M.; Lamboll, R. D.; Booker, E. P.; Wisnivesky Rocca Rivarola, F.; Griffiths, J. T.; Ducati, C.; Menke, S. M.; Deschler, F.; Greenham, N. C. Photon Reabsorption in Mixed $CsPbCl_3$: $CsPbI_3$ Perovskite Nanocrystal Films for Light-Emitting Diodes. *J. Phys. Chem. C* **2017**, *121* (7), 3790−3796.
(29) Gan, Z.; Chen, W.; Yuan, L.; Cao, G.; Zhou, C.; Huang, S.; Wen, X.; Jia, B. External stokes shift of perovskite nanocrystals enlarged by photon recycling. *Appl. Phys. Lett.* **2019**, *114* (1), 011906.
(30) Giovanni, D.; Righetto, M.; Zhang, Q.; Lim, J. W. M.; Ramesh, S.; Sum, T. C. Origins of the long-range exciton diffusion in perovskite nanocrystal films: photon recycling vs exciton hopping. *Light: Sci. Appl.* **2021**, *10* (1), 2.
(31) Seth, S.; Ahmed, T.; Samanta, A. Photoluminescence flickering and blinking of single $CsPbBr_3$ perovskite nanocrystals: revealing explicit carrier recombination dynamics. *J. Phys. Chem. Lett.* **2018**, *9* (24), 7007−7014.

https://doi.org/10.1021/acsphotonics.1c00953
ACS Photonics 2021, 8, 3201−3208